

Article

Automatic Evaluation of an Interwell-Connected Pattern for Fractured-Vuggy Reservoirs Based on Static and Dynamic Analysis

Dongmei Zhang ^{1,*}, Wenbin Jiang ¹, Zhijiang Kang ², Anzhong Hu ¹ and Ruiqi Wang ¹¹ School of Computer Science, China University of Geosciences, Wuhan 430074, China² Petroleum Exploration & Production Research Institute, SINOPEC, Beijing 100081, China* Correspondence: cugzdm@foxmail.com

Abstract: The types of fractured-vuggy reservoirs are diverse, with dissolution holes and fractures of different scales as the main reservoir spaces. Clarifying the connectivity between wells is crucial for improving the recovery rate of fractured-vuggy reservoirs and avoiding problems of poor waterflooding balance and serious water channeling. A traditional dynamic connected model hardly describes the geological characteristics of multiple media, such as karst caves and fractures, which cause multiple solutions from the calculation. The static analysis is the basis for connectivity evaluation. In this study, we designed an intelligent search strategy based on an improved A* algorithm to automatically find a large-scale fractured-vuggy connected path by seismic multi-attribute analysis. The algorithm automatically evaluates the interwell-connected mode and clarifies the relationship between the static connected channel and the fractured-vuggy space configuration. Restricted by various factors, such as seismic identification accuracy, a static connectivity study can hardly determine the filling and half-filling inside the channel effectively, even if it can identify the main connectivity channels. An injection-production response analysis based on dynamic production data can more accurately reflect the reservoir's actual connectivity and degree of filling. This paper further studies dynamic response characteristics based on multifractals combined with production data. To reduce the evaluation uncertainty, we combined the static and dynamic connected analysis results to comprehensively evaluate the main connected modes, such as large fracture connectivity, cavern connectivity, and fractured-vuggy compound connectivity. We use the Tahe oilfield as an example to carry out an automatic evaluation of the connected pattern. The comprehensive evaluation results of the new algorithm were basically consistent with the tracer test results and can better reflect the interwell space-configuration relationship. Our model has certain guiding significance for the adjustment of working measures during waterflooding in fractured-vuggy reservoirs.

Keywords: fractured-vuggy reservoirs; A* algorithm; the fractured-vuggy space configuration; multifractals; connected pattern



Citation: Zhang, D.; Jiang, W.; Kang, Z.; Hu, A.; Wang, R. Automatic Evaluation of an Interwell-Connected Pattern for Fractured-Vuggy Reservoirs Based on Static and Dynamic Analysis. *Energies* **2023**, *16*, 569. <https://doi.org/10.3390/en16010569>

Academic Editor: Reza Rezaee

Received: 24 November 2022

Revised: 28 December 2022

Accepted: 30 December 2022

Published: 3 January 2023



Copyright: © 2023 by the authors. Licensee MDPI, Basel, Switzerland. This article is an open access article distributed under the terms and conditions of the Creative Commons Attribution (CC BY) license (<https://creativecommons.org/licenses/by/4.0/>).

1. Introduction

Fractured-vuggy reservoirs have diverse types and are composed of dissolution pores and fractures of different scales, with strong heterogeneity [1]. As the foundation of waterflooding design, connectivity between fractured-vuggy units is crucial. To avoid the problems of poor waterflooding balance and serious water channeling in some production wells after water injection [2], it is necessary to clarify the water flow direction and injection production parameters of water injection wells [3]. Correctly understanding the spatial morphology and connectivity of dissolution pores between wells is of great significance for optimizing production measures and enhancing oil recovery [4].

Conventional interwell-connectivity analysis methods include both static and dynamic analyses. Static research generally describes the connectivity of reservoirs through structure,

stratigraphic division, and logging curve analysis [5,6]. The fracture is a high permeability channel used to connect the karst cave. The connectivity relationship includes different levels, such as the large-scale fractures, the fracture-cavity, and the micro-fracture system, among which large-scale fractures are the primary way to control the degree of connectivity [7]. Various seismic attributes, such as coherence, seismic dip, and curvature, can explain the different levels of fractures. The coherence attribute can describe the characteristics of large-scale fractures. The maximum curvature attribute identifies minor fractures and folds better. These attributes reflect the distribution characteristics of the interwell geological structure and reservoirs' vertical and plane connectivity [8–10]. Constrained by the limitations of seismic identification accuracy, static research methods [11–13] only preliminarily describe the main connected channels and cannot effectively judge the filling and half-filling degree inside a fracture, which has an impact on its reliability [14].

Dynamic analysis methods use petroleum development data to determine the degree of interwell-connectivity, which reflect the actual conditions of a reservoir more accurately [15]. The analysis methods include tracer testing [16], well testing [17], pressure trend analysis [18], interwell interference [19] and so on. However, there are always problems, such as their effect on normal production, a low water cut or shut-down wells, low efficiency of manual discrimination, and strong subjectivity. Because production data is the result of various engineering and geological factors, numerous academics regard reservoirs as intricate injection-production systems [20]. They assess the degree of interwell connectivity with numerous linear regression models, such as capacitance model, system analysis model, and neural networks. For the first time, Heffer [21] proposed the use of production data to analyze interwell connectivity using the Spearman rank correlation coefficient method to establish connectivity model. However, this method does not consider the time delay of the injected signal. Lagoven et al. [22] examined the attenuation delay of the injected signal when it propagated in the reservoir medium. Soeriawinata et al. [23] considered the injection interaction between wells, combined with the superposition principle, to establish a connectivity inversion model of multiple injection wells. To characterize the influence of the injection volume of water injection wells, Albertoni et al. [24] proposed a multivariate linear regression (MLR) method to establish an injection-production model to quantitatively describe the degree of interwell connectivity. The heterogeneity of the actual reservoir, the high viscosity of a fluid, the distance between wells, and the faults will cause losses to the diffusion and propagation of injection signal. Therefore, information such as shut-down, bottom-hole flow pressure, and relative permeability are introduced to improve the injection-production model [25–27]. Based on a similarity to hydropower, Yousef [28] established a capacitance model (CM) and a series of improved models based on the material balance principle [29–31]. Danial [32] proposed a GCM and CCM model, which can adapt to the change in flowing pressure data and the frequent shut-down of wells in a production system. Mammad [33] introduced a virtual well and proposed a CM production-pseudo well (CMP-PW) model to evaluate the connectivity of tight reservoirs. According to the response of a rectangular pulse signal system, Liu [34] applied a Kalman filtering method to establish a dynamic connectivity model between wells. Given the complexity of the solution process, Zhao [35] improved the system analysis method. In 2016, Zhao [36] proposed and established an interwell connectivity inversion model for the water flooding development of multi-layer reservoirs to solve the problem of non-hierarchical calculation. In addition to the above methods, artificial neural networks combined with sensitivity analysis can also be applied to evaluate interwell connectivity [37,38].

However, assumptions in the above models are often too simple to describe in detail the geological characteristics of multiple media, such as karst caves and cracks. Furthermore, the calculation results are greatly affected by the adjustment measures and have multiple solutions. For fractured-vuggy reservoirs with strong heterogeneity, the key to reducing discrimination uncertainty is determining how to evaluate interwell connectivity by effectively integrating the static and dynamic characteristics of multi-source information. The complex media of carbonate reservoirs have significant spatial scale differences,

discontinuities, and anisotropy characteristics. The geological structure based on pores, fractures, and holes makes the 3D-connected channel search of fractured-vuggy reservoirs complex, causing search efficiency to be low. Based on seismic multi-attribute data that describe the distribution characteristics of the reservoir space at different scales, we design an intelligent search strategy to explore the communication path automatically, which can intuitively describe the static connected channels between the wells. Classic path search algorithms include both non-heuristic and heuristic algorithms. Non-heuristic algorithms include the classic Dijkstra algorithm, artificial potential field method, roadmap method, etc., which generally have poor robustness and low accuracy. Heuristic algorithms can effectively improve search efficiency in combination with practical application scenarios, such as in the case of A*, and improved algorithms are widely used in path search and planning problems in different fields [39–41]. Still, it is challenging to effectively solve a multibranch closed-loop problem in the search process.

To overcome the limitations mentioned above, we propose a number of improvement measures. We categorize our efforts into the three areas listed below:

- We adopt seismic multi-attribute data to depict different types of reservoir bodies and establish an evaluation function that considers the distribution of the geological structure. In addition, we propose an improved A* algorithm to obtain the optimal path by automatically searching for large- and medium-scale fractures and caves.
- Combined with dynamic production data, we use multifractals technique to judge the filling degree of the channel and comprehensively evaluate the main interwell connectivity modes, such as cavern connectivity and fractured-vuggy compound connectivity, which provides effective information for further correction of the static connectivity.
- Based on a typical unit in the Tahe oilfield, we analyzed the tracer test curve and injection-production response production dynamic curve characteristics under different connected modes. The results of the comprehensive automatic evaluation algorithm proposed in this paper are consistent with the tracer test and can better reflect the connectivity between the wells and reveal the potential direction of water flooding.

The remaining parts of the article are arranged as follows. Section 2 introduces three modes of interwell connectivity in fractured-vuggy reservoirs. Section 3 analyzes the static connectivity mode of seismic multi-attribute data in detail. Section 4 analyzes the dynamic connectivity model based on production data. Section 5 evaluates the interwell connectivity model of dynamic integration. Section 6 takes the typical unit of the Tahe oilfield as an example to verify. Section 7 summarizes the performance of the improved model and plans for future research.

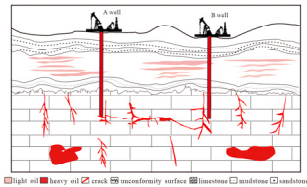
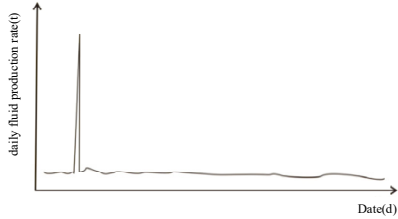
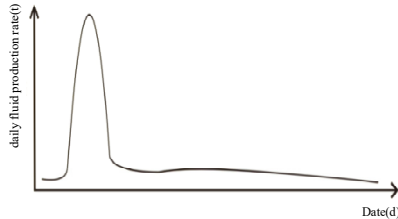
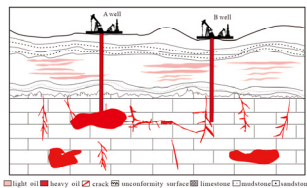
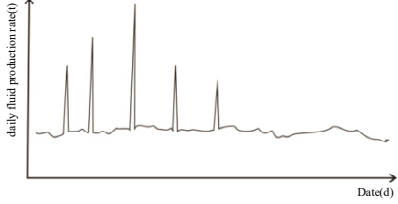
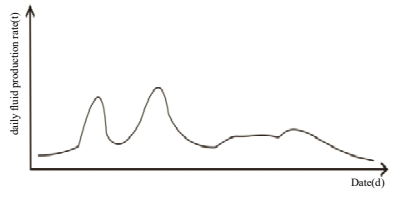
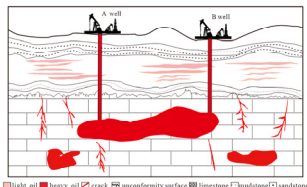
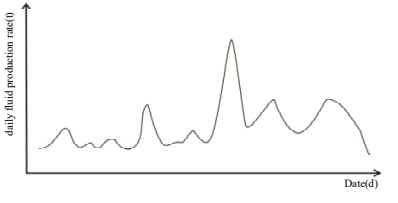
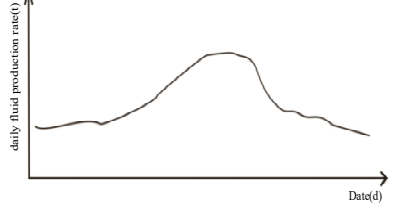
2. Interwell-Connected Mode of Fractured-Vuggy Reservoirs

According to the interwell fractured-vuggy compound relationship in fracture-cavity reservoirs, the interwell-connected mode is mainly divided into three types: large fracture connectivity, cavern connectivity, and fractured-vuggy compound connectivity. More complex connectivity can be regarded as a combination of these three types.

2.1. Large Fracture Connectivity

In fracture-connected mode, a fracture is the main channel and includes large-scale fractures, small-scale, and medium-scale fractures, micro-fractures, and those of other different scales. A large-scale fracture mainly controls the degree of connectivity. Because of the large pressure gradient and high flow rate, the injected water often flows along a large-scale fracture, which is the high permeability zone. The degree of interwell connectivity depends on the orientation, length, and opening of the fracture development. From the tracer concentration curve, we can observe that the output concentration of the injected tracer rises rapidly, controlled by convection to a single peak in a vertical shape. During the water injection period, the dynamic response characteristics between injection–production wells are significant, and the production indexes change dramatically (Table 1) [42].

Table 1. The characteristics of tracer concentration and production under different interwell-connected mode.

inter-well connected mode	connected sketch	tracer concentration characteristics	injection-production response characteristics
fracture connectivity			
fracture - vuggy compound connectivity			
cavern connectivity			

2.2. Fractured-Vuggy Compound Connectivity

Interwell fractured-vuggy compound connected channels include dissolution pores, medium- and small-scale fractures, etc. The degree of connectivity depends not only on the direction, number, and scale of the fractures, but also on the size of the caves and the spatial configuration of the fractured vugs. If the fluid volume in the well is sufficient to balance the pressure fluctuation, the injection-production response and interwell interference are negligible. The tracer is non-uniformly produced, and the concentration curve shows a multi-peak shape with lower peak values and wider wave crests.

2.3. Cave Connectivity

A karst cave is the main part of a connected channel. A smaller range of pressure variation leads to little interference between wells. The curve of tracer concentration shows a slow and parabolic shape, indicating a relatively long tracer production time. Because the production intervals of adjacent production wells are large karst caves, the dynamic response caused by short-term water injection and interwell interference are no obvious.

3. Analysis of Static Connected Mode of Seismic Multi-Attribute Data Fusion

As shown in Figure 1, the fractured-vuggy reservoirs are highly heterogeneous, and we use the 3D seismic data volume to analyze the spatial distribution of karst caves and fractures of different scales. In this study, the coherence attribute describes large-scale fractures, the maximum curvature describes micro-scale fractures, and the root-mean-square (RMS) attributes describe caves. The larger the RMS amplitude attribute value, the greater the possibility that 3D seismic grid points are caves. Similarly, the greater the coherent attribute value, the greater the fracture opening. In this paper, we adopt the A* search strategy to automatically track the optimal interwell path connected by large fractures and caverns and to combine multiple attributes to describe the 3D distribution characteristics of the reservoir.

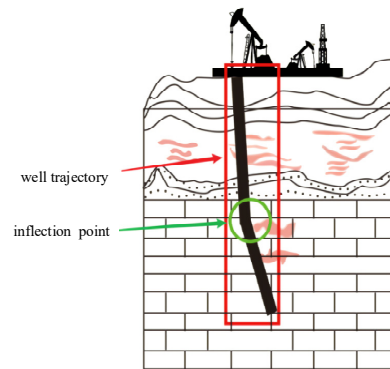


Figure 1. A schematic diagram of the well trajectory.

3.1. A* Path Search Strategy Takes into Account Multiple Seismic Attributes

Due to the complex configuration and discrete distribution of different types of reservoir bodies, we search the connected channels based on the state space. Traditional breadth-first and depth-first searches are blind searches that have low efficiency. The heuristic A* algorithm [43–47] guides the search process by constructing an evaluation function based on the geological characteristics of caves and fractures to obtain a global optimal solution for the connected path. The evaluation function $F(n)$ is divided into two parts: real cost function $G(n)$ and budget cost function $H(n)$. Taking into account the geological characteristics of the reservoir and the main flow direction of the injection fluid, we design real cost evaluation function $G(n)$. In addition, the estimated loss value μ defines the next search strategy.

Definition 1. Evaluation function $F(n)$.

$F(n)$ represents the estimated cost value of the optimal path from the beginning node through node n to destination node e :

$$F(n) = G(n) + \mu \cdot \frac{H_{\max} - H(n)}{H_{\max} - H_{\min}} \quad (1)$$

where μ represents the estimated loss value. H_{\max} and H_{\min} represent the maximum and minimum distance between the adjacent and target node, respectively.

Definition 2. Real cost evaluation function $G(n)$.

$G(n)$ represents the real path cost from the beginning node to the current node n through different types of reservoir body.

$$G(n) = \lambda_1 \cdot X_n - \ln Y_n + \lambda_2 Z_n \quad (2)$$

where λ_1, λ_2 is the weight coefficient. Because of the poor permeability in the matrix, large-scale fractures are the main connected media. The fractures represented by the coherent data X are the main flow direction. The curvature data Z represent micro-scale fractures. The RMS amplitude data Y is processed logarithmically, incorporating multiple seismic attributes designed to match the geological and tectonic characteristics of the fractured-vuggy reservoir.

Definition 3. Budget cost evaluation function $H(n)$.

$H(n)$ is the estimated cost value of the optimal path from the current node n to the target node e :

$$H(n) = |n_x - e_x| + |n_y - e_y| + |n_z - e_z| \quad (3)$$

The evaluation criterion in the formula is the Manhattan distance between the current node n to the target node e .

Figure 2 depicts the search process for the interwell-connected path based on the improved A* algorithm.

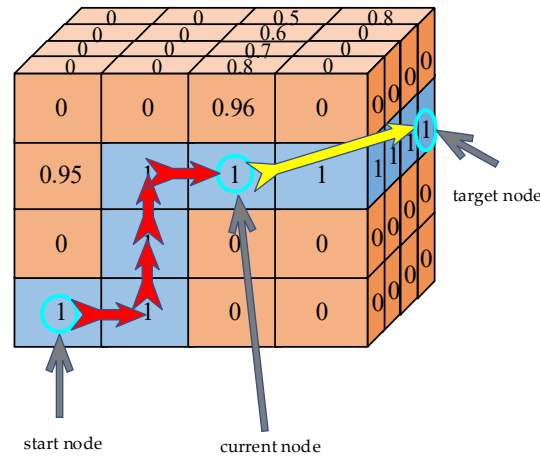


Figure 2. The schematic diagram of interwell-connected path with fused seismic multi-attribute.

To prevent a closed loop in the path search region, we should further analyze the the various paths searched.

Definition 4. Path evaluation function $W(n)$.

$W(n)$ is used to quantify the degree of pros and cons of the path and to calculate the average real cost value of all grid points along the path from the closed-loop entrance to the exit node passes:

$$W(n) = \frac{1}{N} \cdot \sum_{i=pNode}^{next} G(i) \tag{4}$$

where N represents the number of nodes in a certain path in the closed loop; $pNode$ represents the closed-loop entrance node; and $next$ node represents the adjacent node of the current node n . The calculation process of $W(n)$ is shown in Figure 3.

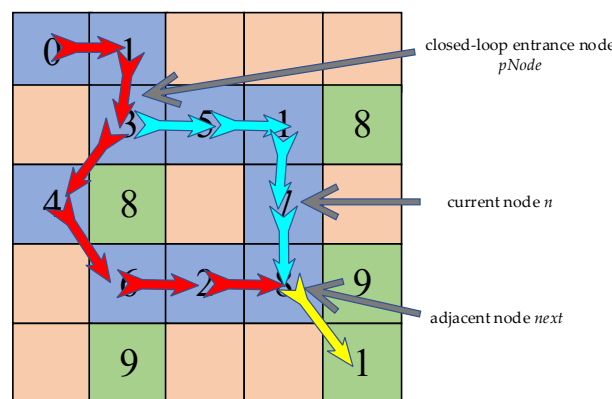


Figure 3. The schematic diagram of closed loop structure of A* algorithm.

3.2. Evaluation of the Static Interwell-Connected Mode

According to the main flow direction, we utilize the A* search strategy based on the seismic multi-attribute analysis to obtain an optimal path between connected well pairs. Furthermore, we analyze whether the reservoir types of the grid nodes flowing through the

path are large fractures or caves and use the evaluation function to determine the connected mode of the path.

Definition 5. Evaluation function $C(p)$ of interwell-connected mode.

$C(p)$ represents the interwell-connected mode of the optimal path, and p represents the ratio of the number of karst caves in the path grid to the total grid number:

$$C(p) = \begin{cases} 0, & 0 \leq p \leq \zeta_1 \\ 1, & \zeta_1 \leq p \leq \zeta_2 \\ 2, & \zeta_2 \leq p \leq 1 \end{cases} \quad (5)$$

where 0 denotes big fracture connectivity, 1 denotes fractured-vuggy compound connectivity, and 2 denotes cavity connectivity; ζ_1 is the fracture connectivity threshold; and ζ_2 is the cavity connectivity threshold.

The evaluation algorithm of static-connected modes based on the fusion of multi-seismic attributes is designed as Algorithm 1:

Algorithm 1: The evaluation algorithm of static-connected modes based on the fusion of multi-seismic attributes

Input: X (coherent data), Y (root mean square amplitude data), Z (maximum curvature data), $start$ (initial node), end (target node)
Output: $connectPath$ (interwell-connected mode)

- 1: **for** X, Y, Z **do**
- 2: Initialize $open$ table of nodes to be extended and $close$ table of nodes extended.
- 3: Add $start$ and end to $open$ table as the initial nodes of the search region.
- 4: Take the maximum point in $open$ table as the current node n based on the evaluation function, which is removed from $open$ table and placed in $close$ table.
- 5: Search connected nodes adjacent to the current node n as set $\{CONNODE\}$.
- 6: Traverse the set $\{CONNODE\}$ to select the $next$ node.
- 7: **if** $next\ node = end$ **then**
- 8: Set $next$ node to the current node.
- 9: Turn to 25.
- 10: **else**
- 11: Turn to 19 by judging whether it is in table $close$.
- 12: **end if**
- 13: Search for the $next$ node in the $open$ table.
- 14: **If** the search succeeds **then**
- 15: Use Formula 4 to evaluate the closed-loop path and set the n node of the optimal path to the $parent$ node of the $next$ node.
- 16: **else**
- 17: Its $parent$ node to n .
- 18: **end if**
- 19: **if** the set $\{CONNODE\}$ is not traversed **then**
- 20: Return to 6.
- 21: **end if**
- 22: **if** the $parent$ table is not empty **then**
- 23: Return to 4.
- 24: **end if**
- 25: Determine whether the current node n is the end node and obtain the optimal path according to the $parent$ node.
- 26: Calculate the reservoir types of each node path.
- 27: Judge and output the interwell-connected mode.
- 28: **end for**

4. Analysis of Dynamic Connected Mode Based on Production Data

Research on static connected mode can only clarify the fractured-vuggy configuration relationship of the connected channel. Based on the response characteristics of the production data and tracer concentration curve, we analyze the interwell energy interference caused by the changing of the working measures, such as with water injection and new well production, to evaluate this different interwell-connected mode.

4.1. Characterization of Interwell Flow Capability Based on a MultiFractals Method

The spatial distributions of dissolved pores and fractures in carbonate reservoirs possess the fractal characteristics of a self-similar structure. The curve of the production data shows abnormal distribution. The permeability between the injection and production wells is proportional to the change range of the production index before and after the water injection. We use the multi-fractal spectrum to describe the change range of the index of production wells, which represents the interwell flow capacity.

Definition 6. Singularity index α_i .

We divide the k -dimensional space R^k ($k = 1, 2, \dots, n$) equally using windows with a side length of δ . $P_i(\delta)$ represents the probability measure of the i -th window. The singularity index α_i is expressed as:

$$\alpha_i = \log P_i(\delta) / \log \delta \quad (6)$$

where $N_\alpha(\delta)$ represents the unit number with the same α value. The relationship between $N_\alpha(\delta)$ and δ is denoted as:

$$N_\alpha(\delta) \sim \delta^{-f(\alpha)} \quad (7)$$

Definition 7. Multi-fractal spectrum $f(\alpha)$.

The multi-fractal spectrum $f(\alpha)$ can be defined as the Hausdorff dimension with the same α -value subset, which describes the change of histogram $N(\delta)$ at $\delta \rightarrow 0^+$, as follows:

$$f(\alpha) = d_H\{x \in \text{supp}P, \alpha(x) = \alpha\} \quad (8)$$

Definition 8. Partition function $\chi_q(\delta)$.

Partition function $\chi_q(\delta)$ describes the distribution characteristics of the multi-fractal spectrum $f(\alpha)$:

$$\chi_q(\delta) = \sum_{i=1}^{N(\delta)} P_i(\delta) \sim \delta^{\tau(q)} \quad (9)$$

where $\tau(q)$ represents a quality index defined as:

$$\tau(q) = \lim_{\delta \rightarrow 0} \log \chi_q(\delta) / \log \delta \quad (10)$$

With a Legendre transformation on q and $\tau(q)$, we can obtain $\alpha(q)$ and $f(\alpha)$. The function is defined as follows:

$$\begin{cases} \alpha(q) = d\tau(q)/dq \\ f(\alpha) = q \cdot \alpha(q) - \tau(q) \end{cases} \quad (11)$$

The width $\Delta\alpha = \alpha_{\max} - \alpha_{\min}$ of the multi-fractal spectrum reflects the non-uniformity of the probability measure distribution.

4.2. MultiFractals Evaluation of Interwell Dynamic-Connected Mode

An adjacent production well has obvious response characteristics, and the production curves change dramatically during waterflooding in fractured-vuggy reservoirs. When the dynamic characteristics become significant, the multi-fractal spectrum becomes wide, which means large fracture connectivity. In contrast, it is likely for a production well to drill into karst caves so that the well is connected by vugs. Other cases can be regarded as similar to fractured-vuggy compound connectivity.

In summary, the evaluation algorithm for the interwell dynamic-connected mode is designed as Algorithm 2:

Algorithm 2: The evaluation algorithm for the interwell dynamic-connected mode

Input: WELLNAME(well name), PTR_EST(production data), ζ_3 (spectral width threshold of fracture connectivity), ζ_4 (spectral width threshold of cave connectivity).

Output: outFile (interwell-connected mode).

1: **for** WELLNAME, PTR_EST, ζ_3 , ζ_4 **do**

2: Read the oil and water production data 60 days after water injection, then set the connectivity threshold, weight factor q , maximum weight factor q_{\max} , time scale sequence δ and length l , and set $j = 0$.

3: Calculate the probability measure $P_i(\delta_j)$ of oil and water production index according to δ_j .

4: Calculate the partition function $\chi_q(\delta_j)$.

5: **if** $j < 1$ **then**

6: $j = j + 1$.

7: Turn to 3.

8: **end if**

9: Calculate quality index.

10: Calculate singularity index α based on Legendre transform.

11: **if** $q < q_{\max}$ **then**

12: $q = q + 1$.

13: Turn to 3.

14: **end if**

15: Calculate multifractal spectrum width $\Delta\alpha = \alpha_{\max} - \alpha_{\min}$.

16: Judge the multi-fractal spectrum width $\Delta\alpha$ according to the set threshold, when it is greater than or equal to ζ_3 , the connected mode is fracture connected.

17: Cave connectivity when less than ζ_4 , the others are regarded as fractured-vuggy compound connectivity.

18: Output the connected mode between injection–production well.

19: **end for**

5. Evaluation of Interwell-Connected Mode Based on Static and Dynamic Fusion

The large depths of fractured-vuggy reservoirs cause seismic signaling to be more complex, including weaker energy. As these issues affect accuracy, high-precision seismic imaging and the recognition of small-scale fracture cavities are challenging. We adopt a static-connected mode-evaluation algorithm based on seismic multi-attribute data and a heuristic search strategy to clarify the main channels. However, the algorithm can cause an unclear understanding of the internal structure and filling degree. To overcome this shortcoming, we further combine the response degree of the production data to revise the static analysis results and to reduce the uncertainty in the connectivity evaluation of deep and ultra-deep complex reservoirs.

The evaluation algorithm is designed as Algorithm 3:

Algorithm 3: The evaluation algorithm

Input: *connectPath*(static interwell-connected mode), *outFile*(dynamic interwell-connected mode).

Output: *result* (comprehensive evaluation results)

```

1: for connectPath, outFile do
2:   if connectPath is a fracture-vuggy compound connected then
3:     Turn to 8.
4:   end if
5:   if connectPath is a cave connected then
6:     Turn to 21.
7:   end if
8:   if outFile is large fracture connectivity then
9:     Judgment of comprehensive evaluation as large fracture connectivity.
10:  end if
11:  if outFile is fracture-cavity compound connectivity then
12:    The partially connected channel is filled.
13:  else
14:    It indicates that the filling is serious.
15:  end if
16:  if outFile is large fracture connectivity or fractured-vuggy compound connectivity then
17:    Judgement of comprehensive evaluation as fractured-vuggy compound connectivity.
18:  else
19:    It indicates that the connected channel is partially filled.
20:  end if
21:  Judge the result as cave connectivity.
22:  Output comprehensive evaluation results.
23: end for

```

6. Case Analysis

The reservoir in Tahe is basically located at a depth of 5564 m. The reservoir intervals are mainly distributed in the Ordovician Yijianfang and Yingshan Formations. The NE–SW and NW–SE are the main directions of fault development in the reservoirs. We used the A injection-production well group as a research object to evaluate the connected mode. The experimental parameters were set to:

$$Threshold = 11000, \zeta_1 = 0.1, \zeta_2 = 0.8, \zeta_3 = 0.5, \zeta_4 = 0.2.$$

6.1. Seismic Data Analysis of Well Group A

Figure 4 shows the spatial combination relationship of the A well group, which is based on the original seismic cross section, the coherent attribute cross section, and the RMS amplitude attribute cross section. As shown in Figure 4a, the original seismic cross section reveals that under the T_7^4 interface, there are apparent “beaded” reflection characteristics in the A well group, which indicates that the reservoirs around these wells are developed. In Figure 4b, the coherent attribute cross section shows the development of fractures between wells and around wells. Different scale fractures are distributed around the W4 well. In Figure 4c, the RMS amplitude attribute cross section describes the distribution of the karst caves in the reservoirs. There are karst caves around the W2 well, and the W3 well encounters small-scale caves.

6.2. Evaluation on the Connectivity Mode of Well Group A

Taking the A well group in the S80 unit as an example, we implemented the connected mode evaluation on the W2, W3, and W4 production wells. Fractures and caves were the main types of reservoir bodies in the unit.

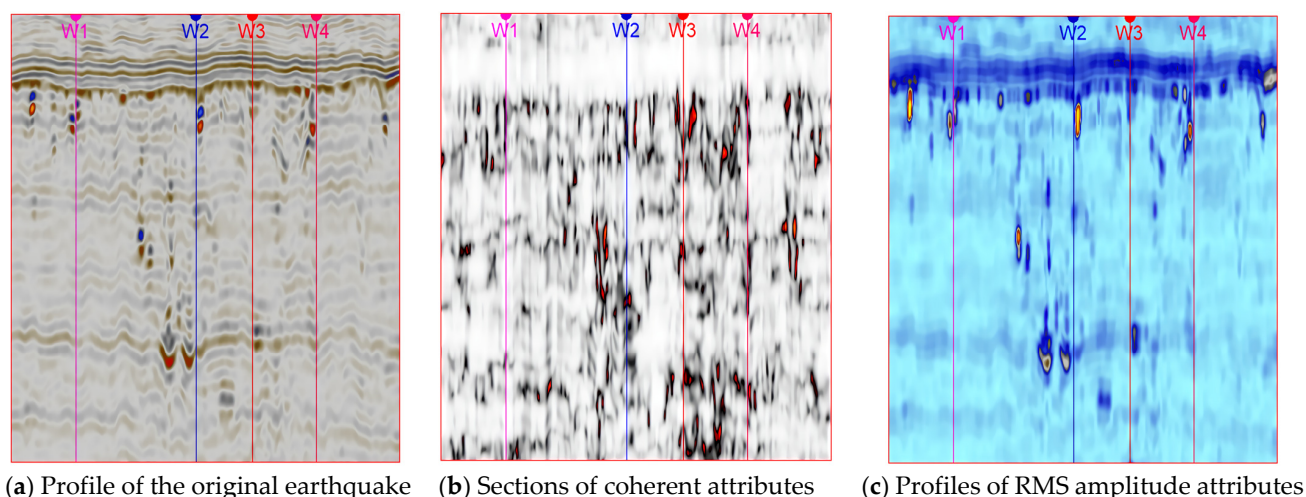


Figure 4. The seismic cross section of A well group.

6.2.1. Evaluation of Static Connected Mode of Seismic Data Fusion

We put forward an improved A* algorithm to search within the A well group. The optimal path is shown in Figure 5, where blue represents the connected path and yellow represents the dissolution holes in the path. In Figure 5, among the three well pairs, only the search path of the W1–W4 well pair were connected along the NW–SE trunk fracture. Dissolved holes developed only around this well pair. The caves ratio in the optimal path means that the specific value of the number of dissolved caves to the total number. W1–W4 well pair’s caves ratio was 0.075. According to the threshold value, the interwell connected mode was determined to be fracture connectivity. The first half of the W1–W3 interwell connected channel overlapped with the search path of W1–W4 and went along the NW–SE trunk fracture direction. W1–W3 well pair’s caves ratio was 0.286 because the karst caves developed in the latter half. According to the threshold, the interwell connected mode was evaluated as fractured-vuggy compound connectivity. The karst caves developed around the W1 well, and the ratio of caves was 0.141. According to the threshold, the interwell connected mode was determined to have fractured-vuggy compound connectivity. This article uses petrel software to visualize the optimal connectivity path. The specific results are shown in Table 2.

Table 2. The results of static well connected mode of A well group based on the ratio of caves.

Evaluating Indicator	Well Pair		
	W1–W2	W1–W3	W1–W4
The ratio of caves and fractures	0.141	0.286	0.075
Interwell-connected mode	fractured-vuggy compound	fractured-vuggy compound	fractured connectivity

As shown in Figure 6, the experiment further depicted the distribution map of regional seismic attributes in the A well group. The coherence attribute can describe the development characteristics of interwell fractures, the curvature attribute can describe small- and medium-scale fractures, and the amplitude attribute can describe the development feature of interwell karst caves. In Figure 6, yellow represents large-scale fractures, gray represents micro-fractures, and red represents caves. Figure 6a shows large-scale fractures along the NW–SE direction in the W1–W4 well pair. The spatial configuration relationships depicted by the coherence and curvature attributes in the A well group are consistent with the main channel features of paths found by the automatic search algorithm.

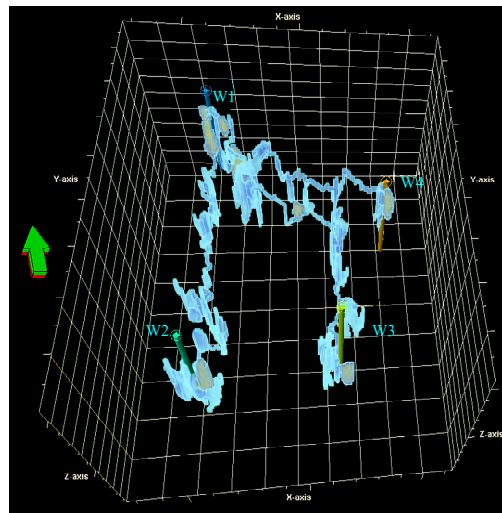
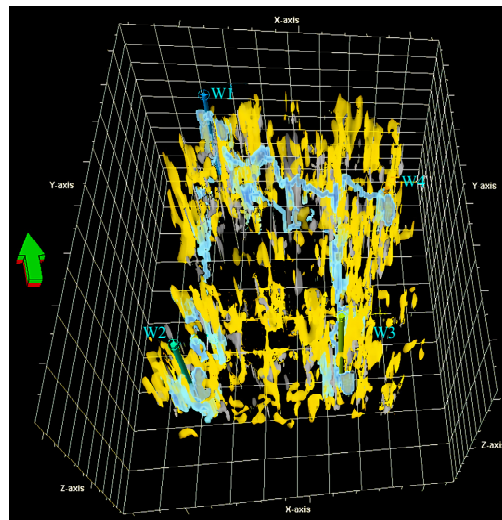
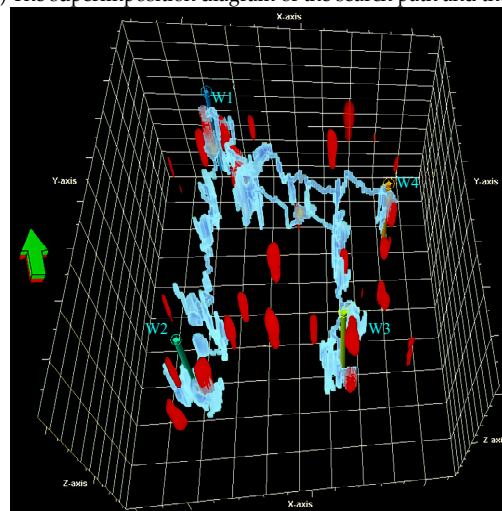


Figure 5. The schematic diagram of the optimal path of A well group.



(a) The superimposition diagram of the search path and the coherence attribute



(b) The superimposition diagram of the search path and the amplitude attribute

Figure 6. The Karst-Fracture Characteristics of A well group.

As shown in Figure 6b, the karst caves distributed around the W1, W2, W3, and W4 wells indicate that the interwell-space configuration relationship of the search path are consistent with the distribution characteristics of the reservoir bodies.

6.2.2. Evaluation of Dynamic-Connected Mode Based on Production Data

We further analyzed the index changes in adjacent production wells after water injection in the W1 well. Taking the W1–W4 injection–production well pair as an example, the daily oil production and daily liquid production of the W4 well continued to increase after water injection in the W1 well in April 2009, with prominent response characteristics. The production curve is shown in Figure 7.

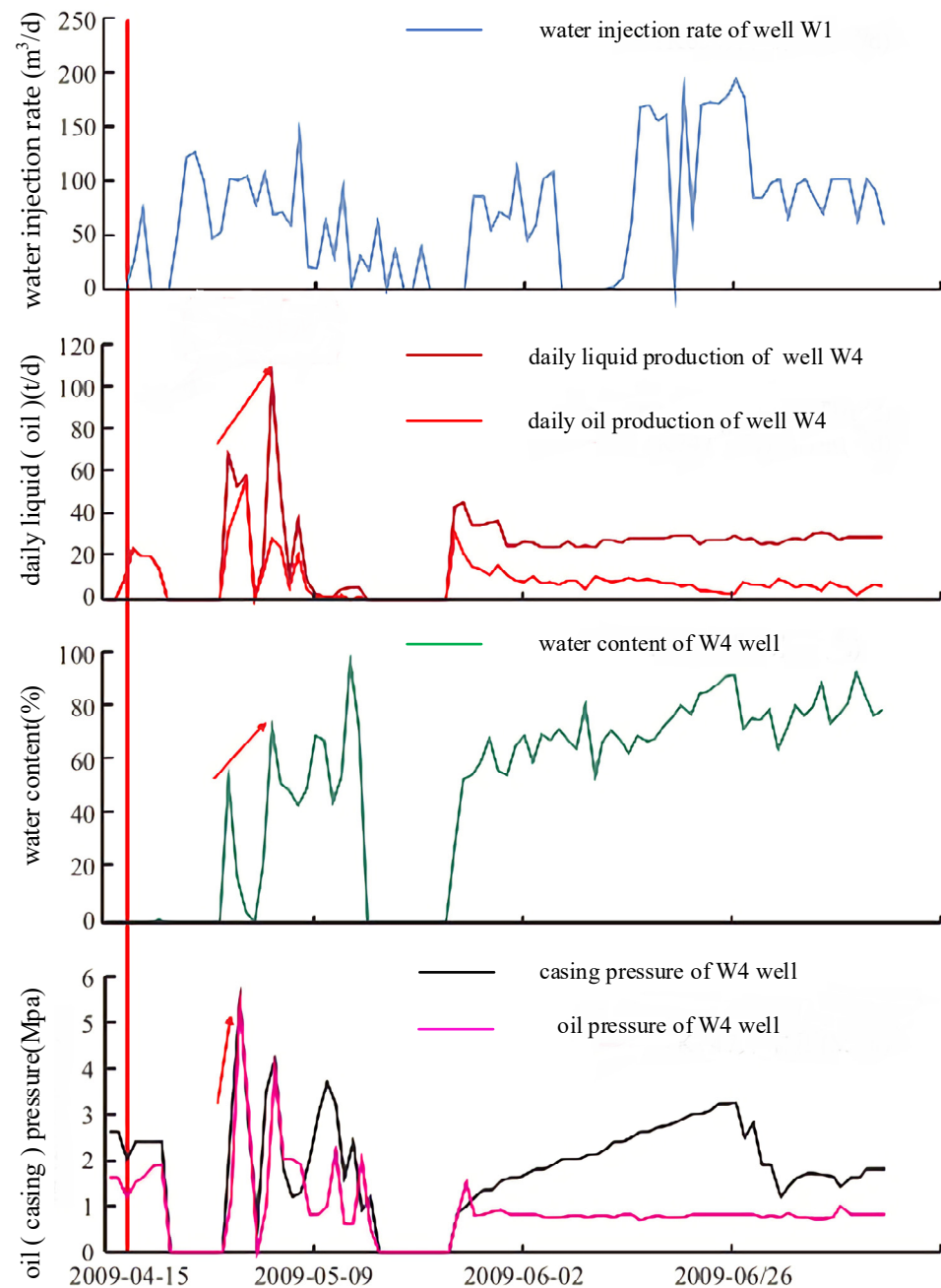


Figure 7. The production curve of W4 well after W1 water injection.

We adopted a multi-fractal method to calculate the change degree of the daily oil production and daily water production index of the connected well group A 60 days after water injection. The results are shown in Table 3.

Table 3. The injection–production response characteristics of A well group.

Production Well	Well Pair	W3	W4
Evaluating Indicator			
Evaluating Indicator		0.22383	0.60584
Daily water production	0.35648	0.27013	0.71909

In Table 3, the production index of the W4 well changes sharply during the water injection and has significant dynamic response characteristics, so it was judged as fracture connectivity according to the algorithm threshold. The production indexes of the W2 and W3 wells changed gently and were judged as fractured-vuggy compound connectivity.

6.3. Automatic Evaluation of Interwell-Connected Pattern Based on Static and Dynamic Analysis

In summary, the connected modes of W1 to the W2, W4, and W3 well groups were consistent with the results based on the static and dynamic data. Furthermore, we tested and analyzed the tracer in the A well group. This group injected the BY-2 tracer on 23 April 2009, and it took 172 days until 12 October 2009. The concentration curve and monitoring results of the tracer in the connected production wells are shown in Figure 8 and Table 4.

Table 4. The tracer test results of A well group.

Production Well	Background Concentration (cd)	Breakthrough Time (d)	Breakthrough Concentration (cd)	Propulsion Speed (m/d)
W2	18.07	30	40.8	77.22
W3	19.93	19	54.2	126.33
W4	23.80	8	136.7	219.53

The tracer output concentration indicates whether there is a hypertonic channel. The higher the output concentration, the stronger the connectivity. The tracer curve's shape and peak number indicate the fluid flow mode in the reservoirs and the number of connected channels. From Figure 8 and Table 4, we can observe that the tracer concentration curve of well W2 can be characterized as vertical rising in the early stage and then a parabolic shape. With a breakthrough time of 30 days, a breakthrough concentration twice the background concentration, and a low advanced speed of 77.22 m/d, there are characteristics of dispersion and diffusion, which means the compound connectivity of cracks and holes between the W2 and W1 wells. The shape of the tracer concentration curve of the W4 well shows a lead hammer rise. With a breakthrough concentration of 5.7 times the background concentration, a breakthrough time of eight days, and a fast advanced speed, it indirectly indicates that the wells are connected along the direction of the NW–SE trunk fault. The reservoirs in this direction possessed good permeability and were the dominant seepage channels. The tracer passed through the W4 well and reached the W3 well, so we obtained a tracer breakthrough time of 19 days, an advancing speed around 126.33 d/t, and a breakthrough concentration 2.7 times the background concentration. The latter curve contains multiple parabolic shapes, which indicates fractured-vuggy compound connectivity between the W3 and W1 wells. The tracer curve in the three wells coincided with the connected mode and the ratio parameter of caves, as calculated by the algorithm.

We propose an automatic algorithm for evaluating the interwell-connected mode in fractured-vuggy reservoirs based on static and dynamic fusion, which is consistent with the interwell-spatial configuration relationship shown in the tracer test. The new method is more convenient and faster because the tracer test is affected by daily production and cannot be judged when a well is shut off and contains no water.

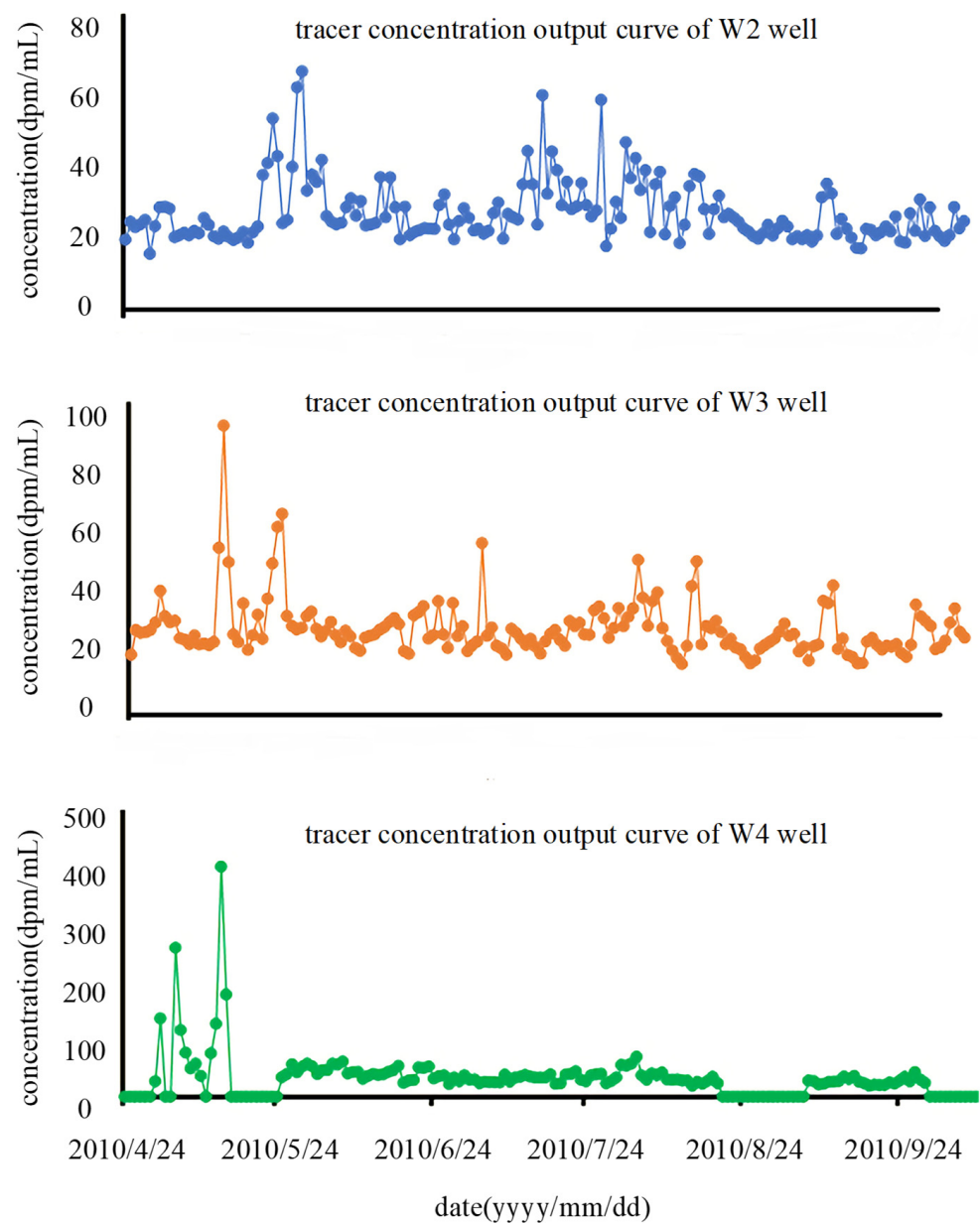


Figure 8. The tracer concentration curve of A well group.

7. Conclusions

Aiming at the problems existing in traditional connected mode judgment, we adopted seismic multi-attribute data to describe the static connected channel and spatial configuration relationship. In addition, we combined the multi-fractal spectrum after water injection of production data to judge the channel permeability, which reduces the uncertainty of the quantitative evaluation of complex fractured reservoir connectivity. Our approach is an automatic algorithm for evaluating the interwell connected mode in fractured-vuggy reservoirs based on static and dynamic fusion. The examination of a typical injection-production well group of the Tahe area showed that the results from our approach were consistent with the interwell spatial configuration relationship of the tracer test. The new algorithm can effectively reduce the uncertainty of interwell connectivity relationship evaluation. In addition, it is significant for the adjustment of working measures during waterflooding in fractured-vuggy reservoirs.

Considering the heterogeneity of fractured-vuggy reservoirs and the multiple solutions of connected channels, we will further study the multi-path search strategy combined with a multi-objective evolutionary algorithm.

Author Contributions: Conceptualization, D.Z.; Methodology, D.Z.; supervision, Z.K.; Writing—original Draft, D.Z.; Formal analysis, W.J., R.W. and A.H.; Validation, W.J. and A.H.; Investigation, W.J.; Writing—review and editing, W.J.; Data curation, Z.K.; Software, R.W.; Visualization, R.W.; experiment, W.J., R.W. and A.H. All authors have read and agreed to the published version of the manuscript.

Funding: This work was supported in part by the National Natural Science Foundation of China Joint Fund Key Project (grant number U19B6003) and in part by the National Science and Technology Major Project “Fractured-cavity Reservoir Enhanced Oil Recovery Technology” (grant number 2016zx05014-003).

Data Availability Statement: The data presented in this study are available on request from the corresponding author. The data are not publicly available due to [data is confidential].

Conflicts of Interest: We declare that we have no known competing financial interest or personal relationship that could have appeared to influence the work reported in this paper.

References

- Li, Y. Development theory and method of fractured-vuggy carbonate reservoir in Tahe Oilfield. *J. Pet.* **2013**, *34*, 115–121.
- Liu, Z.; Sun, Y.; Li, Q.; Guo, W. Characteristics of gas-water flow during gas injection in two-dimensional porous media with a high-permeability zone. *J. Hydrol.* **2022**, *607*, 127588–127599. [[CrossRef](#)]
- Xie, S.; Liu, R.; Tan, T. Research on water flooding characteristics of channel sand reservoir in tahe oilfield and improvement of water flooding technology. *Xinjiang Oil Gas* **2019**, *15*, 66–72+4–5.
- Gilyazov, A.A.; Salimov, A.O.; Vadulina, N.V. On improving the efficiency of flooding to increase oil recovery during oil fields development. *J. Phys. Conf. Ser.* **2021**, *1889*, 022074. [[CrossRef](#)]
- Yang, J.; Cheng, Q.; Li, J.L.; Liu, Z.C. Interwell connectivity of fractured-vuggy reservoirs in Block 4 of Tahe Oilfield, Tarim Basin. *Pet. Nat. Gas Geol.* **2012**, *33*, 484–489+496.
- Li, X.B.; Li, X.H.; Rong, Y.S.; Peng, X.L.; Wang, K.K. The application of seismic attributes in the connectivity analysis and water injection development of carbonate fractured-vuggy reservoirs in Tahe Oilfield. *Oil Gas Geol. Recovery* **2014**, *21*, 65–67+71+115.
- Lu, X.B. Heterogeneity of karst fracture-cavity carbonate reservoir. *Pet. Geol. Xinjiang* **2003**, *04*, 360–362.
- Hou, J.G.; Ma, X.Q.; Liu, Y.M.; Zhao, B. Research on multi-class and multi-scale modeling methods for fractured-vuggy carbonate reservoirs: A case study of Ordovician reservoirs in Block 4 of Tahe Oilfield. *Geol. Front* **2012**, *19*, 59–66.
- Hu, X.Y.; Li, Y.; Quan, L.S.; Kong, Q.Y.; Wang, Y.; Lv, X.R. A three-dimensional geological modeling method for carbonate fractured-vuggy reservoirs—a case study of the ordovician reservoir in block 4 of Tahe oilfield. *Pet. Nat. Gas Geol.* **2013**, *34*, 383–387.
- Hu, X.Y.; Yuan, X.C.; Hou, J.G.; Quan, L.S. Reservoir modeling method for multi-scale karst facies-controlled carbonate fractured-vuggy reservoir. *J. Pet.* **2014**, *35*, 340–346.
- Lv, X.R.; Li, H.K.; Wei, H.H.; Si, Z.N.; Wu, X.W.; Bu, C.P.; Kang, Z.J.; Sun, J.F. Classification and characterization method for multi-scale fractured-vuggy reservoir zones in carbonate reservoirs: An example from Ordovician reservoirs in Tahe oilfield S80 unit. *Oil Gas Geol.* **2017**, *38*, 813–821.
- Lu, X.B.; Zhao, M.; Hu, X.Y.; Jin, Y.Z. Three-dimensional modeling method for carbonate fractured-vuggy reservoirs: A case study of Tahe Ordovician fractured-vuggy reservoirs. *Pet. Exp. Geol.* **2012**, *34*, 193–198.
- Cui, S.Y.; Di, Y. Numerical Simulation of Fractured-Vuggy Reservoir Based on Assumption of Gravity Segregation. *J. Basic Sci. Eng.* **2020**, *28*, 331–341.
- Chen, X.H.; Zhong, W.L.; He, Z.H. Reservoir detection based on time-frequency domain Teager main energy. *Oil Geophys. Explor.* **2011**, *46*, 434–437+500+328.
- Zhang, M.L.; Guo, F.; Lin, J.H. The Application of Dynamic Development Data in Low-Permeability Reservoir Water Flooded Layer Identification. In Proceedings of the 2014 International Conference on Energy Science and Applied Technology (ESAT 2014 V733), Daqing, China, 21 December 2014; pp. 169–172.
- Zhou, L.M.; Guo, P.; Liu, J.; Liu, L.N. Using tracer data to discuss the interwell connectivity of Tahe fractured-vuggy reservoirs. *J. Chengdu Univ. Technol.* **2015**, *42*, 212–217.
- Guo, Q.; Guo, K.L. Well Test Analysis Method and Application of Carbonate Reservoir in Tahe Oilfield. *J. Yangtze Univ. Sci. Technol. Vol.* **2007**, *4*, 151–152.
- Xie, X.H.; Yan, C.H.; Lai, S.Y.; He, G.H.; Luo, Z. Study on Interwell Connectivity of Fractured-vuggy Carbonate Reservoir in Block 6 of Tahe Oilfield. *Pet. Geol. Eng.* **2013**, *27*, 103–105.
- Miu, L.L.; Di, S.Y. Quantitative analysis of inter-well connectivity in interference like well testing. *Oil-Gas Field Surf. Eng.* **2014**, *33*, 16–17.

20. Zhao, H.; Kang, Z.J.; Zhang, Y. Connectivity calculation method for characterizing formation parameters and oil-water dynamics between wells. *Pet. J.* **2014**, *35*, 922–927.
21. Heffer, K.J.; Fox, R.J.; McGill, C.A. Novel Techniques Show Links between Reservoir Flow Directionality, Earth Stress, Fault Structure and Geomechanical Changes in Mature Waterfloods. *SPE J.* **1997**, *2*, 91–98. [[CrossRef](#)]
22. Lagoven, S.A.; Lake, L.W. Reservoir Characterization Based on Tracer Response and Rank Analysis of Production and Injection Rates. In Proceedings of the International Reservoir Characterization Technical Conference, Tulsa: American Association Petroleum Geologists, Houston, TX, USA, 2–4 March 1997; pp. 359–367.
23. Soerawinata, T.; Kelkar, M. Reservoir Management Using Production Data. In Proceedings of the Spe Mid-Continent Operations Symposium, Oklahoma City, OK, USA, 28 March 1999.
24. Albertoni, A.; Lake, L.W. Inferring interwell connectivity only from well-rate fluctuations in waterfloods. *SPE Reserv. Eval. Eng.* **2003**, *6*, 6–16. [[CrossRef](#)]
25. Jensen, J.L.; Lake, L.W.; Al-Yousef, A. *Interwell Connectivity and Diagnosis Using Correlation of Production and Injection Rate Data in Hydrocarbon Production*; Texas A&M University; Texas A & M Engineering Experiment Station: College Station, TX, USA, 2007. [[CrossRef](#)]
26. Gentil, P.H. *The Use of Multilinear Regression Models in Patterned Waterfloods: Physical Meaning of the Regression Coefficients*; The University of Texas at Austin: Austin, TX, USA, 2005.
27. Dinh, A.; Tiab, D. Inferring Interwell Connectivity from Well Bottomhole-Pressure Fluctuations in Waterfloods. In Proceedings of the Production and Operations Symposium, Oklahoma City, OK, USA, 31 March–3 April 2007; pp. 874–881, SPE-106881-PA.
28. Yousef, A.A.; Gentil, P.; Jensen, J.L.; Lake, L.W. A capacitance model to infer interwell connectivity from production-and injection-rate fluctuations. *SPE Reserv. Eval. Eng.* **2006**, *9*, 630–646. [[CrossRef](#)]
29. Lake, L.W.; Liang, X.; Edgar, T.F.; Yousef, A.A.; Sayarpour, M.; Weber, D. Optimization of oil production based on a capacitance model of production and injection rates. In Proceedings of the Hydrocarbon Economics and Evaluation Symposium, Dallas, TX, USA, 1–3 April 2007.
30. Sayarpour, M.; Zuluaga, E.; Kabir, C.S.; Lake, L. The use of capacitance–resistance models for rapid estimation of waterflood performance and optimization. *J. Pet. Sci. Eng.* **2009**, *69*, 227–238. [[CrossRef](#)]
31. Yousef, A.A.; Jensen, J.L.; Lake, L.W. Integrated interpretation of interwell connectivity using injection and production fluctuations. *Math. Geosci.* **2009**, *41*, 81–102. [[CrossRef](#)]
32. Kaviani, D.; Jensen, J.L.; Lake, L.W. Estimation of interwell connectivity in the case of unmeasured fluctuating bottomhole pressures. *J. Pet. Sci. Eng.* **2012**, *90*, 79–95. [[CrossRef](#)]
33. Mirzayev, M.; Riazi, N.; Cronkright, D.; Jensen, J.L.; Pedersen, P.K. Determining well-to-well connectivity in tight reservoirs. In Proceedings of the SPE/CSUR Unconventional Resources Conference, Calgary, AB, Canada, 20–22 October 2015.
34. Liu, F.; Mendel, J.M.; Nejad, A.M. Forecasting injector/producer relationship from production and injection rates using an extended Kalman filter. *Spe J.* **2009**, *14*, 653–664. [[CrossRef](#)]
35. Zhao, H.; Kang, Z.; Zhang, X.; Sun, h.; Cao, L. A physics-based data-driven numerical model for reservoir history matching and prediction with a field application. *SPE J.* **2016**, *21*, 2175–2194. [[CrossRef](#)]
36. Zhao, H.; Kang, Z.J.; Sun, H.T.; Zhang, X.S.; Li, Y. Interwell connectivity inversion model for water-flooding multilayer reservoirs. *Pet. Explor. Dev.* **2016**, *43*, 99–106. [[CrossRef](#)]
37. Panda, M.N.; Chopra, A.K. An integrated approach to estimate well interactions. In Proceedings of the SPE India Oil and Gas Conference and Exhibition, New Delhi, India, 17 February 1998.
38. Demiryurek, U.; Banaei-Kashani, F.; Shahabi, C.; Wilkinson, F.G. Neural-network based sensitivity analysis for injector-producer relationship identification. In Proceedings of the Intelligent Energy Conference and Exhibition, Amsterdam, The Netherlands, 25–27 February 2008.
39. Zhao, C.Y.; Jiang, H.; Xu, M.Z.; Man, W.J.; Yang, W.M.; Chen, F.M. Application of Improved A * Algorithm in Unmanned Ship Path Planning. *J. Zhejiang Univ. Technol.* **2022**, *50*, 615–620.
40. Guo, Y.Y.; Yuan, J.; Zhao, K.G. Robot path planning based on improved A~* algorithm and dynamic window method. *Comput. Eng. Sci.* **2022**, *44*, 1273–1281.
41. Jiang, Y.Y.; Zhang, Y.Y. Improvement of 8-neighborhood Node Search Strategy A~* Algorithm for Path Planning. *J. Electron. Meas. Instrum.* **2022**, *36*, 234–241.
42. Zhang, D.M.; Kang, Z.J.; Chen, X.D.; Jiang, X.W. *Quantitative Evaluation of Connectivity between Wells in Fractured-Vuggy Reservoirs*; University of Geosciences Press: Wuhan, China, 2020.
43. Chen, G.Y.; Yu, S. Improved A* multi robot bilevel path planning algorithm. *Comput. Eng. Appl.* **2022**, 1–10. Available online: <http://kns.cnki.net/kcms/detail/11.2127.TP.20220523.1532.002.html> (accessed on 10 January 2022).
44. Wang, X.D.; Zhang, H.W.; Liu, S.; Wang, J.L.; Wang, Y.H.; Shangguan, D.H. Path planning of scenic spots based on improved A* algorithm. *Sci. Rep.* **2022**, *12*, 1320. [[CrossRef](#)] [[PubMed](#)]
45. Shi, J.; Su, Y.; Bu, C.; Fan, X. A mobile robot path planning algorithm based on improved A*. *J. Phys. Conf. Series. IOP Publ.* **2020**, *1486*, 032018. [[CrossRef](#)]

46. Zhao, P.; Lei, X.Y.; Chen, B.Z.; Yang, J.Y. TI-A* based multi-robot dynamic planning and coordination method. *J. Syst. Simul.* **2019**, *31*, 925–935.
47. Zhang, C.C.; Fang, J.D. Path planning of autonomous mobile robot based on directional weighted A* algorithm. *J. Comput. Appl.* **2017**, *37*, 77–81.

Disclaimer/Publisher's Note: The statements, opinions and data contained in all publications are solely those of the individual author(s) and contributor(s) and not of MDPI and/or the editor(s). MDPI and/or the editor(s) disclaim responsibility for any injury to people or property resulting from any ideas, methods, instructions or products referred to in the content.